

# FUSE AND IUE SPECTROSCOPY OF THE PROTOTYPE DWARF NOVA ER URSA MAJORIS DURING QUIESCENCE

GIANNINA GUZMAN<sup>1</sup>, EDWARD M. SION<sup>1</sup>, AND PATRICK GODON<sup>1,2</sup>

<sup>1</sup>Department of Astrophysics & Planetary Science, Villanova University, Villanova, PA 19085, USA

<sup>2</sup>Henry A. Rowland Department of Physics & Astronomy, The Johns Hopkins University, Baltimore, MD 21218, USA

## ABSTRACT

ER Ursae Majoris is the prototype for a subset of SU UMa-type dwarf novae characterized by short cycle times between outburst, high outburst frequency, and “negative” superhumps. It suffers superoutbursts every 43 days, lasting 20 days, normal outbursts every 4 days and has an outburst amplitude of 3 magnitudes. We have carried out a far ultraviolet (FUV) spectral analysis of ER UMa in quiescence, by fitting *Far Ultraviolet Spectroscopic Explorer* (FUSE) and *International Ultraviolet Explorer* (IUE) spectra with model accretion disks and high gravity photosphere models. Using the Gaia parallax distance and an orbital inclination of 50°, we find that during the brief quiescence of only four days, the accretion rate is  $7.3 \times 10^{-11} M_{\odot}/\text{yr}$ , with the ER UMa white dwarf contributing 55% of the FUV flux and the accretion disk contributing the remaining 45% of the flux. The white dwarf in ER UMa is markedly hotter (32,000 K) than the other white dwarfs in dwarf novae below the CV period gap which have typical temperatures  $\sim 15,000$  K. For a higher inclinations of 60 to 75 degrees, the accretion rates that we derive are roughly an order of magnitude higher  $1 - 3 \times 10^{-10} M_{\odot}/\text{yr}$ .

**Keywords:** — dwarf novae, cataclysmic variables — stars: white dwarfs — stars: individual (ER UMa)

## 1. INTRODUCTION

ER Ursae Majoris is the prototype system of a subclass of SU UMa type dwarf novae. Like SU UMa systems they exhibit two types of outbursts: normal and superoutbursts. These superoutbursts show superhumps that are ruled by tidal instabilities. In the canonical view of the CVs below the period gap, the mass-transfer rate from the secondary star is governed by the rate of angular momentum loss due to gravitational wave emission, which happens to be strongly correlated to the orbital period. Yet, there were some systems that challenged the traditional SU UMa classification due to their frequency of outbursts, superoutbursts and suspected unusually high mass-transfer rates for the dwarf novae below the CV period gap. Once ER UMa was discovered in the Palomar Sky Survey as an ultraviolet-excess object (Green et al. 1986), along with a handful of similar systems, it was clear that they belonged to a new subclass of SU UMa systems (e.g. Iida 1994; Kato & Jayacura 1995; Kato et al. 1999). After the observation of dwarf nova outbursts in the system (Iida 1994), it was seen that ER UMa is characterized by an extremely high outburst frequency and short supercycles (Kato et al. 1999), suggesting a higher mass transfer rate than other SU UMa systems. During a superoutburst, ER UMa was confirmed to have ‘negative’ superhumps, a behavior observed since the 1990’s. Negative superhumps are a dynamic behavior of the system in which the superhumps have a shorter period than the orbital period (Ohshima et al. 2018), and displayed retrograde precession (Harvey et al. 1995; Patterson et al. 1997; Patterson 1999; Skillman et al. 1999; Wood & Burke 2007; Montgomery 2012). This is thought to be due to an eccentric tilted disk. Some theories suggest that ER UMAs are simply an evolutionary stage of classical novae, through studies of the recently sub-classified ER UMa system: BK Lyncis (Patterson et al. 2012).

The published orbital and physical parameters of ER UMa are given in Table 1 along with the literature references. Dubus et al. (2018) take an inclination of  $45 \pm 10^\circ$  for ER UMa, but the observation of sharp absorption lines in the optical may indicate that the system may have a low inclination (Szkody et al. 1996). The correct orbital inclination of ER UMa is unknown. Szkody et al. (1996) cite the line widths, small equivalent widths and low radial velocity amplitude of ER UMa as indicating a low inclination. On the other hand, Thorstensen et al. (1997) found, using the

**Table 1.** Orbital and Physical Parameters of ER UMa

Parameter	Value	Reference
$P$	0.06366 d	<a href="#">Thorstensen et al. (1997)</a>
$d$	374 pc	Gaia
$i$	$18 - 50^\circ$	<a href="#">Szkody et al. (1996)</a> ; <a href="#">Dubus et al. (2018)</a>
$E(B - V)$	0.01	
$M_{\text{wd}}$	$1.0 \pm 0.2 M_\odot$	this paper
$M_2$	$0.10 M_\odot$	<a href="#">Dubus et al. (2018)</a>
$q$	0.100	<a href="#">Ohshima et al. 2014</a>

double convolution method, that the separation of the Gaussian peaks is 1260 km/s and the radial velocity of the WD is 48 km/sec. If one assumes  $1M_\odot$  for the WD and  $0.1M_\odot$  for the secondary star and applies Kepler’s 3rd Law, the corresponding inclination is  $i \sim 50^\circ$ . However, the uncertainties in this inclination value are large. First, the  $H_\alpha$  radial velocity curve of the white dwarf obtained over four nights shows a large scatter. Thorstensen et al.(1997) caution that, in cases where there is an independent check on the gamma velocity and radial velocity semi-amplitude  $K$  of the WD, these two quantities rarely reflect the true dynamical motion of the WD. Furthermore, different emission lines may form in different parts of the accretion disk and thus it cannot be assumed that they manifest the true dynamical motion of the white dwarf. Therefore, in view of the lack of a truly reliable value for the inclination, we carry out here an analysis of ER UMa FUV spectra for a range of values of the inclination, namely  $i = 18^\circ, 41^\circ, 65^\circ$ , and  $70^\circ$ .

In section 2, we present the FUV spectroscopic observations. In section 3, we present the details of our accretion disk and high gravity photospheric models, and we describe our analysis and model fitting results. Finally in section 4, we summarize our conclusions.

## 2. FAR ULTRAVIOLET SPECTROSCOPIC OBSERVATIONS

In 1995, ER UMa was observed with *IUE* and seven spectra were obtained during its 43 days supercycle ([Szkody et al. 1996](#)). The data show large flux changes through the cycle with corresponding large spectral lines changes. The *IUE* spectrum presented here was obtained during quiescence on April 17 and exhibits mainly emission lines. The data were collected through the LARGE aperture, LOW dispersion, short wavelength camera: SWP54455. No data were collected through the long wavelength camera, hence we do not have long wavelength coverage of the quiescent state of ER UMa. The *IUE* spectrum of ER UMa in quiescence has a wavelength coverage of  $\sim 1150\text{--}2000 \text{ \AA}$ . The exposure time is 8,700 s, or about  $\sim 1.6$  orbital period. The *IUE* observation log for the SWP54455 data is in Table 2.

On January 15, 2004, ER UMa was observed in quiescence with *FUSE* ([Froning et al. 2012](#)) with the LWRS (30 arcsec) aperture for 15 consecutive *FUSE* orbits. However, only 10 exposures had valid data. The *FUSE* spectrum presented here consists of the co-added 10 good exposures, totalling 30,625 s of good exposure time. The total (raw) *FUSE* observation time was 13.5 hr, or about  $\sim 8.8$  orbital period. The *FUSE* observation log for the 10 exposures is in Table 2.

All spectral data were retrieved from the on-line MAST archive and were all processed and calibrated by the pipelines. For the *FUSE* observations we used our suite of IRAF procedures, FORTRAN programs, and Linux shell scripts to post-process the data from the 8 different channels into one final spectrum (see [Godon et al. 2012](#), e.g. taking care of the “worm”), with a wavelength coverage  $904\text{--}1188 \text{ \AA}$ . Due to the hydrogen cut-off (Lyman series/jump) the spectrum starts around  $914 \text{ \AA}$ .

The *FUSE* and *IUE* spectra were de-reddened assuming  $E(B-V) = 0.01$  and using the extinction curve of [Fitzpatrick & Massa \(2007\)](#).

In Figs. 1 and 2, we display the dereddened *FUSE* and *IUE* spectra, respectively, the continuum fluxes levels in both spectra matched up in the wavelengths region where they overlap between 1170 and 1180. Thus, the two spectra combined together cover a broader wavelength range than the *FUSE* or *IUE* spectrum alone. This wider wavelength coverage samples more of the SED of ER UMa which helps to achieve more accurate model fits. Figs. 1 and 2 show the strongest lines identified for both spectra.

Table 3 highlights the characteristics of the identified lines in the *FUSE* spectrum intrinsic to CVs, and the lines due to the ISM have been labeled as such (e.g. [Godon et al. 2012](#)). Some characteristic lines are not clearly identifiable in the spectral plot and therefore are not included in the table.

All the sharp emission lines (H I and He II) in the *FUSE* spectrum of ER UMa are all likely due to daylight reflected

**Table 2.** Observation Log

Telescope	Data ID	Date (UG) yyyy-mm-dd	Time (UT) hh:mm:ss	Exp. Time (s)
<i>IUE</i>	SWP54455	1995-04-17	22:04:26	8700
<i>FUSE</i>	D90514002	2004-01-15	08:56:38	806
<i>FUSE</i>	D90514003	2004-01-15	09:42:18	2249
<i>FUSE</i>	D90514004	2004-01-15	10:38:29	1169
<i>FUSE</i>	D90514005	2004-01-15	11:30:07	3615
<i>FUSE</i>	D90514006	2004-01-15	13:06:43	4119
<i>FUSE</i>	D90514007	2004-01-15	14:43:52	4204
<i>FUSE</i>	D90514008	2004-01-15	16:24:22	4178
<i>FUSE</i>	D90514009	2004-01-15	18:02:43	4274
<i>FUSE</i>	D90514011	2004-01-15	19:57:13	3161
<i>FUSE</i>	D90514012	2004-01-15	21:45:09	2910

inside the telescope (more than 50% of the observation took place during the “daytime” of the *FUSE* telescope, i.e. when it is not in the shade of the Earth). The very broad emission lines of O VI (1032 & 1038 Å) and C III (1175 Å) are from the hottest component of the system located in the inner disk and exhibit a strong Keplerian broadening. There are possibly additional broad emission lines (e.g. C III 977 Å) especially in the very short wavelength region ( $\lambda < 950$  Å, higher ionization species such as S VI, N IV) which might be broad enough to merge together to form the continuum observed in the range  $\sim 920 - 945$  Å. The spectrum displays many sharp and shallow ISM absorption lines mostly from molecular hydrogen (rotational and vibrational energy levels) and from some metals such as N I, C II, Si II, Fe II, and Ar I. The S IV, Si III & IV and C III absorption lines are from ER UMa as they are not as sharp. Taking into account that the FUSE spectrum was obtained over a period of time of the order of the several binary orbital periods, the fact that we do see narrow absorption lines from the source (but not as narrow as the ISM lines) is an additional argument in favour of the low inclination.

Table 4 shows the identifiable lines from the IUE spectrum. The very strong S IV emission doublet is due to the high temperature of the hot component in the system. C IV is in emission too, and could be associated with a disk corona or the boundary layer. Finally, there is also a distinct blend of Al III lines, which, because of their apparent strength, could be due to a suprasolar abundance of Al III, perhaps accumulated from the thermonuclear ashes of previous novae that are either being fed back to the white dwarf, or are brought to the surface of the white dwarf from below by a process such as radiative acceleration or forced (shear) convective mixing during outburst.

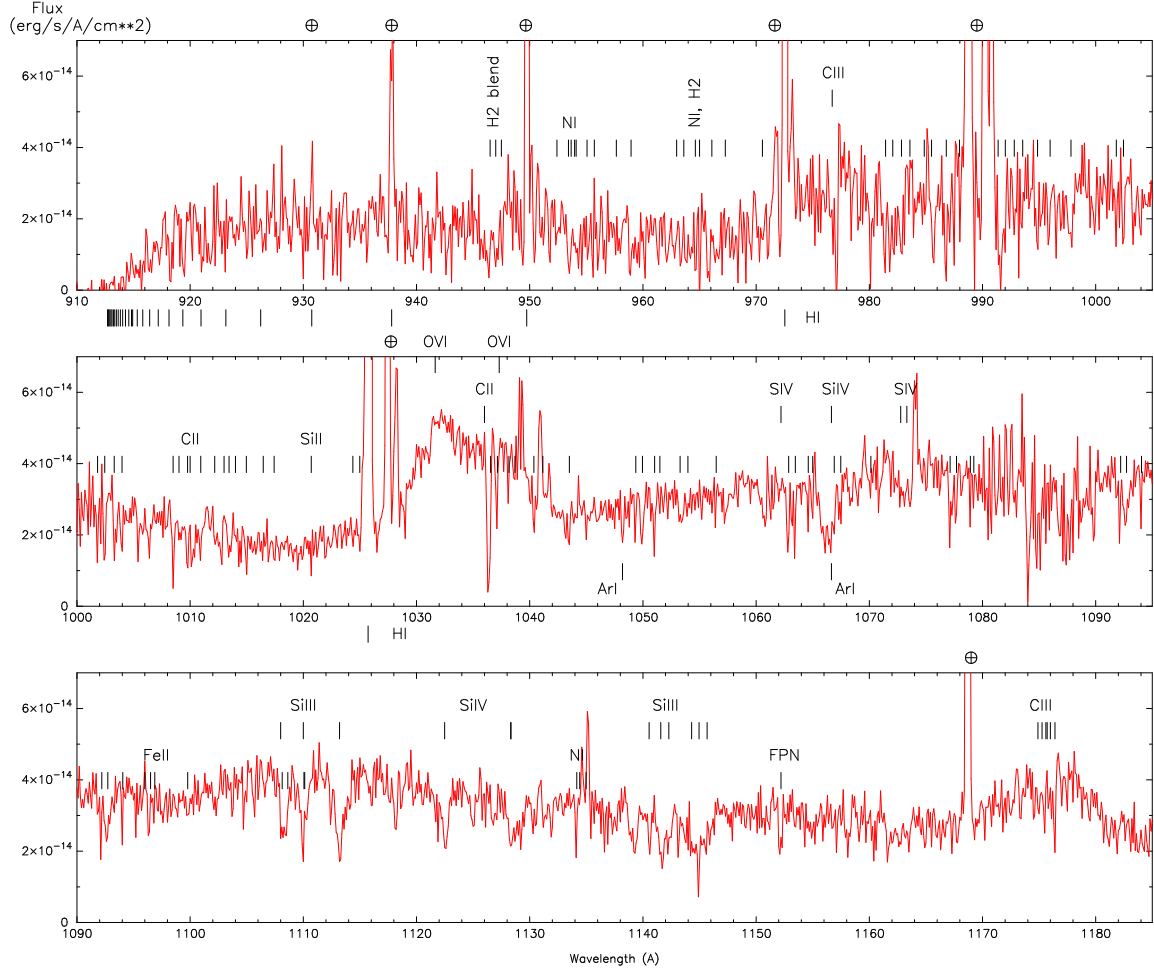


**Figure 1.** *FUSE* spectrum of ER UMa (flux versus wavelength) obtained during quiescence. The sharp emission lines (H I and He II) are all due to daylight reflected inside the telescope, and only the broad emission lines of O VI (1032 & 1038 Å) and C III (1175 Å) are positively identified as originating from the source. ISM absorption lines have been marked with tick marks in the middle of each panel and consist mostly of molecular hydrogen. Additional ISM absorption lines of N I, C II, Si II, Fe II, Ar I have also been marked. The Si IV, Si III & IV and C III absorption lines are from ER UMa. The air glow emission lines have been annotated above each panel with a cross inside a circle, and correspond mainly to the Lyman hydrogen series which have been annotated below each panel. FPN is a detector fixed pattern noise artifact.

**Table 3.** FUSE Identified Line Features

Feature	Wavelength	Emission/Absorption	Likely Source
H I	913-9	e	daylight
H I	923.2	e	daylight
H I	926.2	e	daylight
H I	930.7	e	daylight
H I	937.8	e	daylight
H I	949.7	e	daylight
H I	972.5	e	daylight
H <sub>2</sub> blend	946-948	a	ISM
N I	953-955	a	ISM
N I	954-956	a	ISM
H <sub>2</sub> and N I	962-971	a	ISM
C III	~976.8	a	ISM
N III	~989.6	e	daylight
He II	991.8	a	daylight
C II	1010	a	ISM
Si II	1021	a	ISM
O VI	1031.9	e broad	Stellar
C II	1036	a	ISM
O VI	1037.6	e broad	Stellar
Ar I	1048.5	a	ISM
Si IV	1066.	a	Stellar
Ar I	1066.8	a	ISM
S IV	1073.4	a + e?	Stellar
Si III	1108-1113	a	Stellar
P V ?	1117	a	Stellar
Si IV	1122.5+1128	a	Stellar
P V ?	1128	a	Stellar
N I	1135	e	daylight
Si III blend	1140.7-1145.9	a	Stellar
FPN	1152.6		Fixed Pattern Noise
He II	1168	e	daylight
C III	1175	a/e?	Stellar

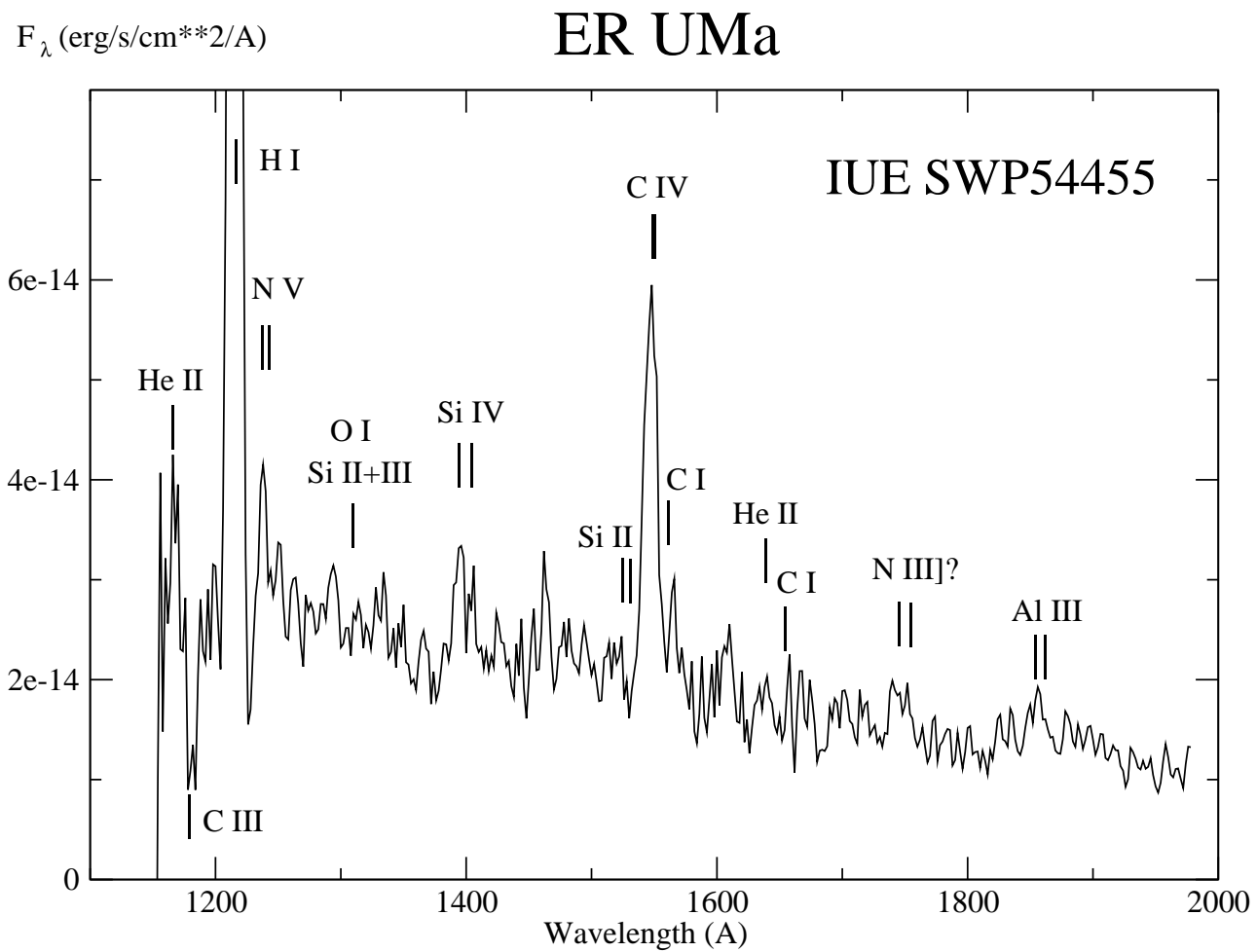


**Figure 2.** IUE spectrum of ER UMa (Flux versus wavelength) obtained during dwarf nova quiescence with line identifications.

**Table 4.** IUE Identified Line Features

Feature	Wavelength	Emission/Absorption	Likely Source
He II	1168	e	stellar?
C III	1175	a	stellar
H I	1225	e	airglow
N V	1239-1243	e/a	stellar
O I + S II+III	~1300	a	stellar
Si IV	1394, 1403	e	stellar
Si II	1527, 1533	a	stellar
C IV	1548-51	e	stellar
C I	1561	e/a	stellar
He II	1640	e?	stellar
C I	~ 1657	e/a?	stellar
Al III	1671	e/a?	stellar
N III]	1747,1754	e	stellar
Al III	1854, 1862	e	stellar

### 3. SYNTHETIC SPECTRAL MODELING AND ANALYSIS.

The dereddened spectra were fitted with both disk and photosphere models in order to extract certain values for analysis such as white dwarf mass, accretion rate, and inclination angle. The model accretion disks were implemented from the optically thick, steady state, disk model grid for solar composition better known as the ‘standard disk model’ (Wade and Hubeny 1998). For these models, the accretion disk’s outermost radius  $R_{out}$  is chosen in such a way that the effective temperature is around 10,000 K. Disk annuli beyond  $R_{out}$  are neglected because they contain cooler zones with very little contribution to UV flux in the FUSE and IUE SWP spectral range.

The Wade & Hubeny DISK models cover the following combination of inclination angle  $i$ , white dwarf mass  $M_{wd}$ , and mass accretion rate  $\dot{M}$ :  $i = 18, 41, 60, 75, \& 81$  deg;  $M_{wd} = 0.35, 0.55, 0.80, 1.03, 1.21 M_{\odot}$ ,  $Log(\dot{M}) = -8.0, -8.5, -9.0, -9.5, -10.0, -10.5 M_{\odot}/yr$ . For the photosphere models, we used TLUSTY (Hubney 1988) and SYNSPEC (Hubney and Lanz 1995) to construct a solar composition, white dwarf, stellar photospheres grid. The temperatures range from 12,000 K to 60,000 K in 1,000 K to 5,000 K step sizes. The stellar surface gravity is set to agree with the white dwarf mass accretion disk models above. The projected stellar rotation rate is varied from 50 km/s to 500 km/s, in steps of 50km/s.

#### 3.1. Low Inclination Models

Our disk and photosphere modeling starts with the parameters listed in Table 1. Having the Gaia distance removes one free parameter. Optical spectroscopic observations (Szkody et al. 1996; Thorstensen et al. 1997) reveal narrow line widths and low radial velocities in ER UMa ( $K_1 \sim 50$ km/s), which may be indicating the system orbital inclination may be low. Therefore, we first restricted the range of disk inclination angles in our disk modeling to be 18 degrees. The mass ratio  $q = 0.10$  was taken from the study of the period of Stage A (positive) superhumps by Ohshima et al. (2014). We included a white dwarf component in the model fits described below, not only to assess its flux contribution in quiescence relative to an accretion disk but also because its inclusion should help improve the fits to the observed absorption lines that are unaccounted for in the disk model itself.

With the Gaia distance  $d = 374$  pc, a disk inclination angle  $i = 18^{\circ}$ , we fit the observed combined *FUSE* + *IUE* spectrum with a white dwarf mass  $M_{wd} \approx 1.0 \pm 0.2 M_{\odot}$ , with a temperature of  $T_{wd} = 30,000 \pm 5000$  K, and a disk with a mass accretion rate  $\dot{M} = 10^{-10.5} - 10^{-10} M_{\odot}/yr$ . Fitting the *FUSE* and *IUE* spectra alone gives the same results.

In Figs. 3 & 4 we display the best-fit accretion disk + WD model to the combined *FUSE* + *IUE* spectrum of ER UMa. For convenience the *FUSE* spectral range is shown in Fig.3 and the *IUE* spectral range is shown in Fig.4. This model has a white dwarf mass  $M_{wd} = 1.03 M_{\odot}$ , a mass accretion rate  $\dot{M} = 3.26 \times 10^{-11} M_{\odot}/yr$  and a white dwarf surface temperature  $T_{wd} = 32,000$  K. The white dwarf, with a radius of 5,611 km ( $Log(g) = 8.6377$ ), contributes 55% of the FUV flux and the accretion disk contributes 45%. To fit the absorption lines, the projected stellar rotational velocity  $V_{rot} \sin i$  was set to 100 km/s.

In the very short wavelengths of the *FUSE* range, Fig.3, the model has too little flux to fit the observed continuum flux level. Models with a higher WD temperature and/or higher mass accretion rate provides an adequate flux level there, but the distance obtained is far too large and the model steep slope does not agree with the *IUE* slope of the spectrum. These models also generate different absorption lines that were not observed. These models had to be discarded. Instead, it is more likely that the flux continuum in the very short wavelengths of *FUSE* is due to broad emission lines of N IV ( $\sim 923$  Å), S VI (933 & 945 Å) merged together.



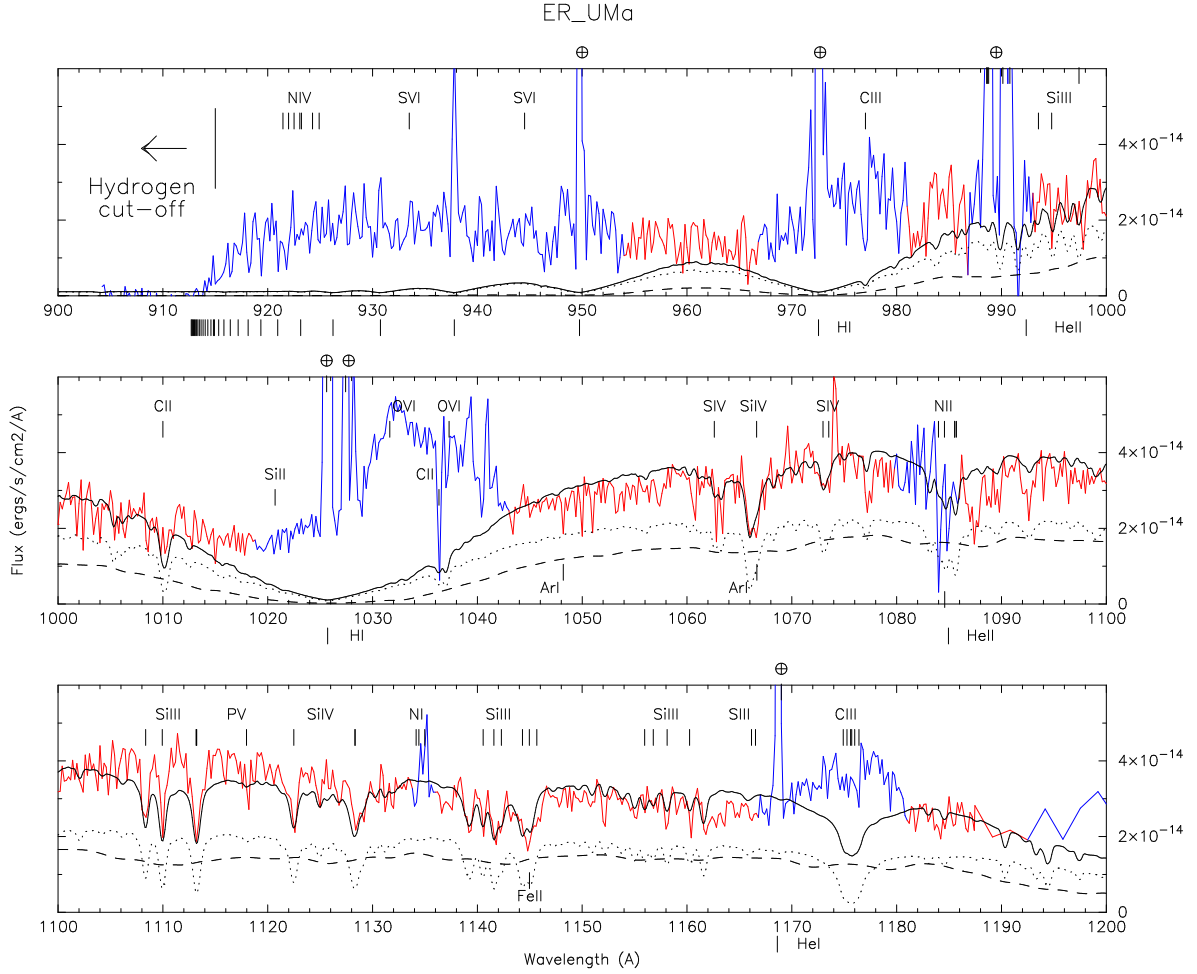


**Figure 3.** A model fit (solid black line) to the de-reddened combined *FUSE* + *IUE* spectrum of ER UMa in quiescence (solid red line). The model is a combined 32,000 K WD (dotted black line) plus an accretion disk (dashed black line) with a mass accretion of  $3.26 \times 10^{-11} M_{\odot}/\text{yr}$ . The WD mass is  $M_{\text{wd}} = 1.03 M_{\odot}$ , the inclination of the disk is 18 degrees, and the distance has been set to 374 pc. The strong emission lines and regions affected by airglow have been masked and are in blue. In order to match the absorption lines, the projected stellar rotational velocity has been set to 100 km/s.

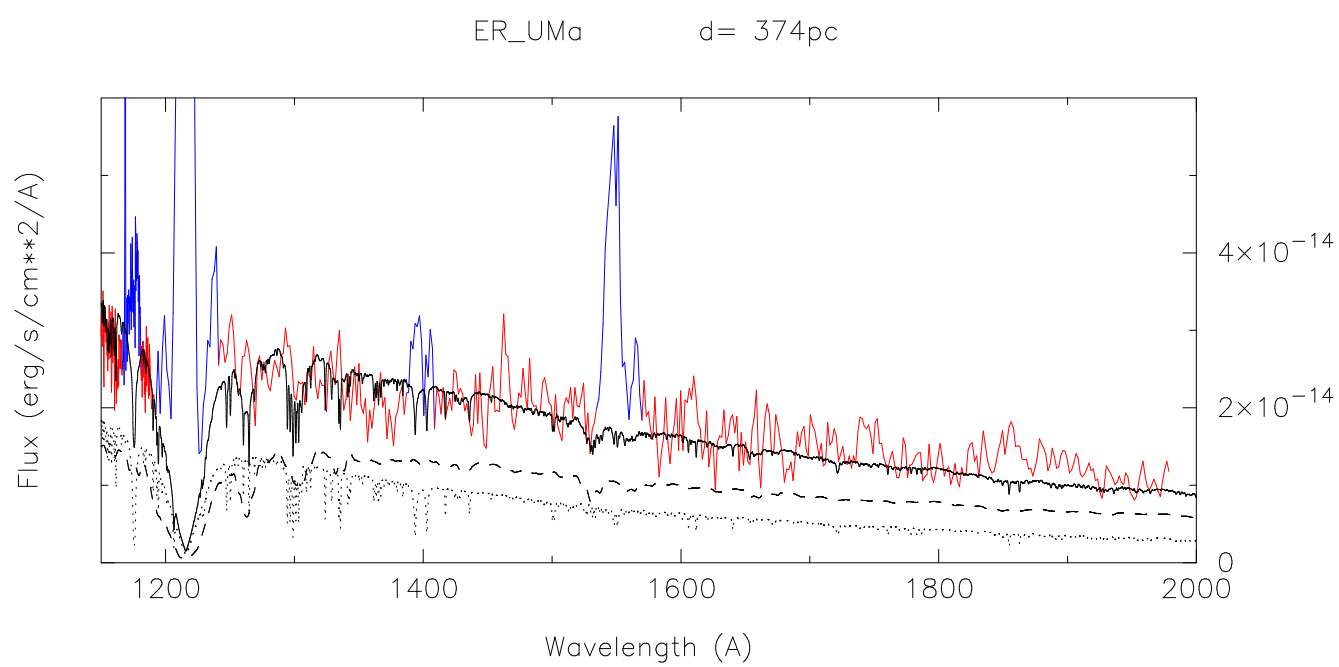


**Figure 4.** Same as in Fig.3 displaying the *IUE* spectral range.

### 3.2. High Inclination Models

In Fig. 5, we display the best-fit model accretion disk to the FUSE spectra of ER UMa. This model has a white dwarf mass of  $M_{\text{wd}} = 1.03M_{\odot}$ , an inclination angle of 75 degrees and yields an accretion rate of  $\dot{M} = 3 \times 10^{-10} M_{\odot}/\text{yr}$ . The scale-factor-derived distance (344 pc) is well within the error bars of the Gaia parallax distance. Next we sought the best-fit models to the combined FUSE plus IUE spectrum. This led to a best-fit disk model to the entire FUSE + IUE SWP spectrum displayed in Fig. 6 where again the white dwarf mass is  $M_{\text{wd}} = 1.03M_{\odot}$ , but now the disk inclination is 60 degrees, the accretion rate is  $\dot{M} = 1 \times 10^{-10} M_{\odot}/\text{yr}$  and the scale-factor-derived distance is 370 pc. In Fig. 7, the combined spectrum is best-fitted with a disk model having  $M_{\text{wd}} = 1.03M_{\odot}$ , disk inclination angle of 75 degrees and an accretion rate of  $\dot{M} = 3 \times 10^{-10} M_{\odot}/\text{yr}$ , corresponding to a scale factor-derived distance of 378 pc. In both of the best fits to the combined spectra, the flux contribution of a white dwarf, although a minor contributor to the continuum flux, does help to improve the accuracy of the fit by accounting for the observed absorption lines. We note also that the best fits to the combined (FUSE + IUE) spectrum give essentially the same accretion rate as that derived for the FUSE-only spectrum in Fig.5.

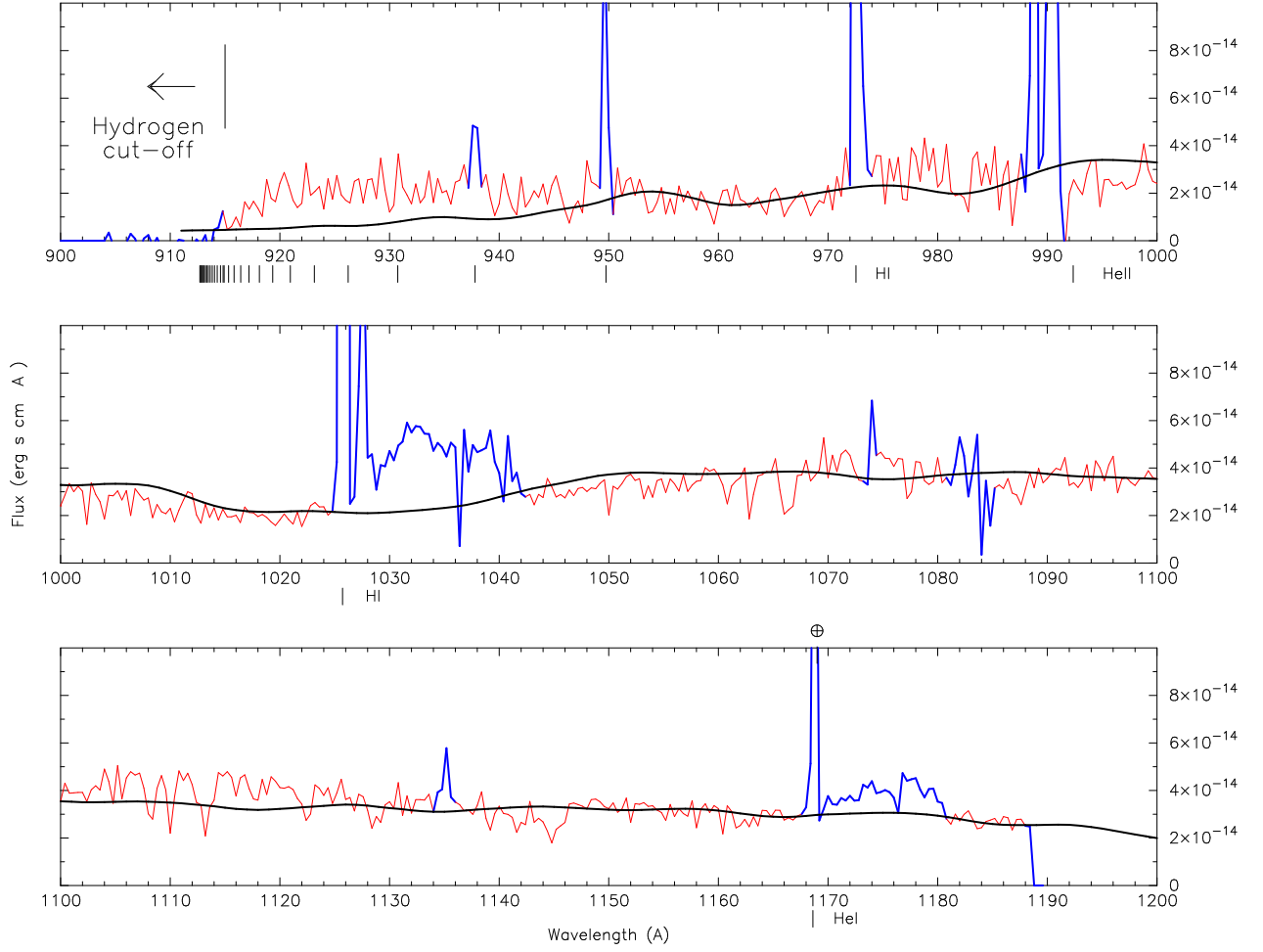


**Figure 5.** The best-fit accretion disk model to the de-reddened FUSE spectrum (alone) of ER UMa in quiescence. The solid blue line is the disk model with  $M_{\text{wd}} = 1.03M_{\odot}$ , inclination angle of 75 degrees, and an accretion rate of  $\dot{M} = 3.0 \times 10^{-10}M_{\odot}/\text{yr}$ , giving a scaled distance of 340 pc.

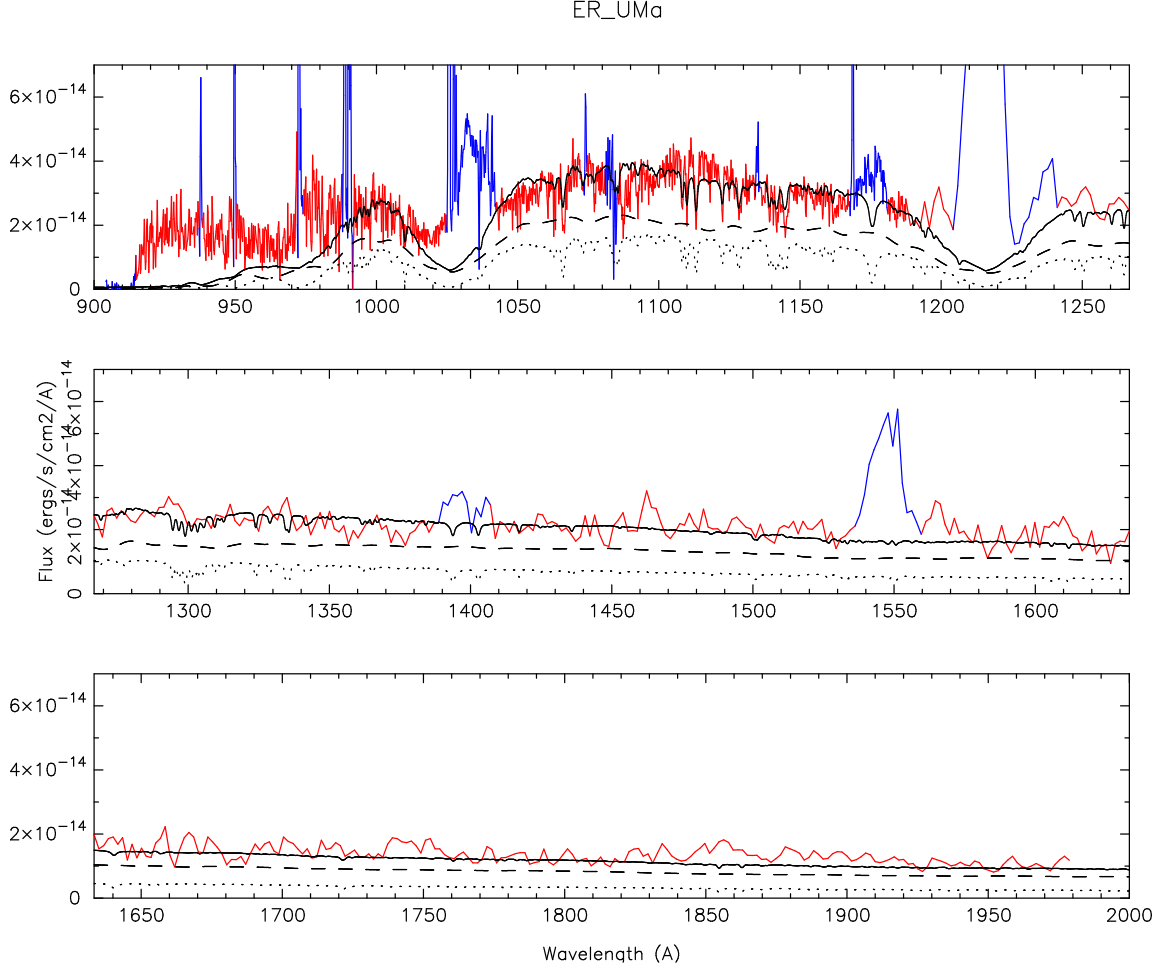


**Figure 6.** The best-fit combined accretion disk plus white dwarf photosphere model to the de-reddened FUSE + IUE spectrum of ER UMa in quiescence. The solid line is the total model flux (disk plus white dwarf), the dashed line is the accretion disk flux, the dotted line is the flux contribution of the white dwarf. The disk parameters are  $M_{\text{wd}} = 1.03M_{\odot}$ , disk inclination angle of 60 degrees, and an accretion rate of  $\dot{M} = 1 \times 10^{-10}M_{\odot}/\text{yr}$ . The white dwarf has  $T_{\text{eff}} = 30,000\text{K}$ . The model distance is 370 pc

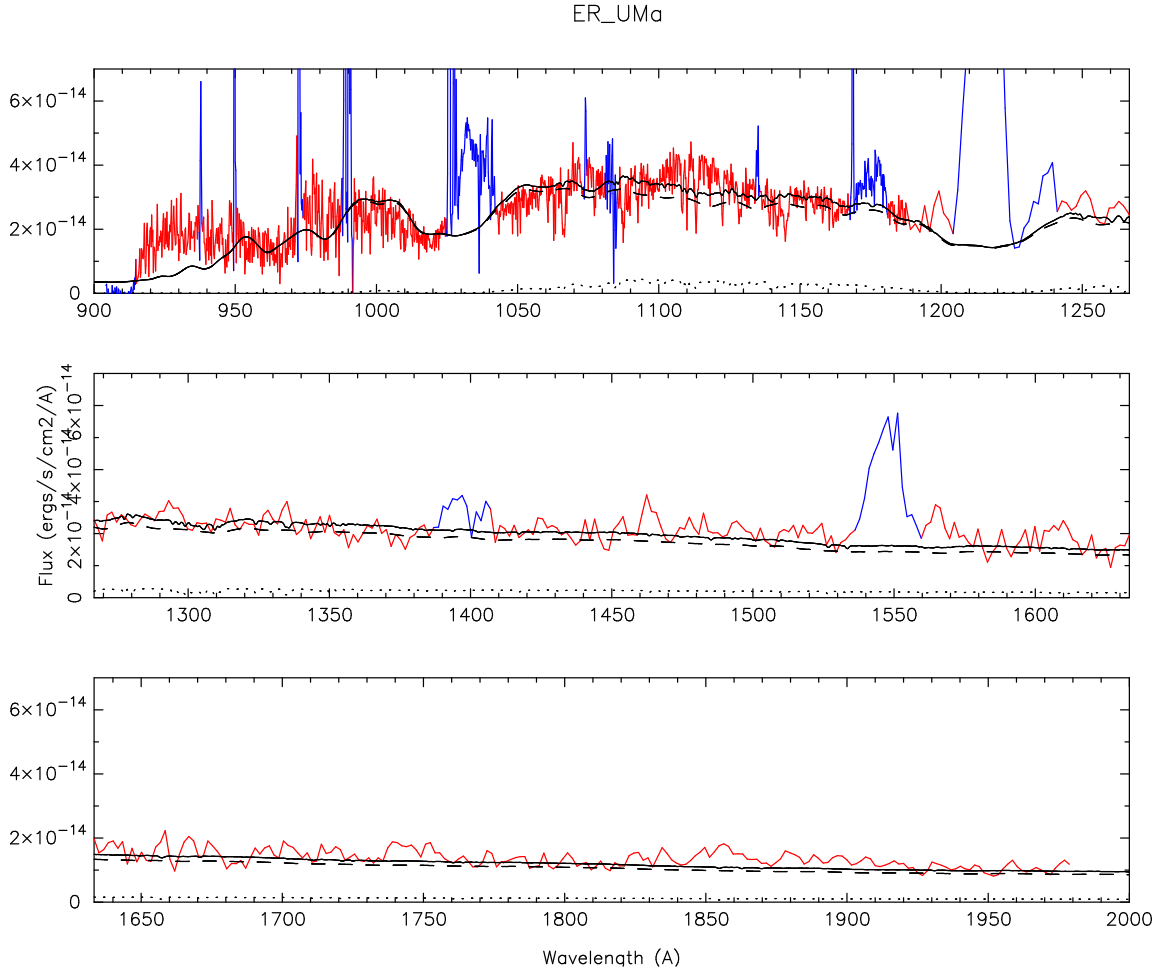


**Figure 7.** The best-fit combined accretion disk plus white dwarf photosphere model to the de-reddened FUSE + IUE spectrum of ER UMa in quiescence. The solid line is the total model flux (disk plus white dwarf), the dashed line is the accretion disk flux, the dotted line is the flux contribution of the white dwarf. The disk parameters  $M_{\text{wd}} = 1.03M_{\odot}$ , disk inclination angle of 75 degrees, and an accretion rate of  $\dot{M} = 3 \times 10^{-10}M_{\odot}/\text{yr}$ . The white dwarf has  $T_{\text{eff}} = 22,000\text{K}$ . The model distance is 378 pc.

**Table 5.** Synthetic Spectra Model Fit Results

Model #	$M_{\text{wd}}$ $M_{\odot}$	$T_{\text{wd}}$ 1000 K	$\dot{M}$ $M_{\odot}/\text{yr}$	$i$ deg	$d$ pc	Fig #
1	1.03	32	$3.26 \times 10^{-11}$	18	374	3,4
2	1.03	—	$7.0 \times 10^{-11}$	41	381	—
3	1.03	32	$4.5 \times 10^{-11}$	41	367	—
4	1.03	30	$1.0 \times 10^{-10}$	60	370	6
5	1.03	—	$3.0 \times 10^{-10}$	75	344	5
6	1.03	22	$3.0 \times 10^{-10}$	75	378	7

#### 4. SUMMARY AND CONCLUSION

In Table 5, we tabulate the best-fit accretion disk models for the two cases of high and low inclination. For an intermediate inclination of  $i = 50^\circ$ , we ran models with  $i = 41^\circ$  and  $60^\circ$  which nicely bracket  $50^\circ$ . Interpolating between the  $41^\circ$  disk model and the  $60^\circ$  disk model, we estimate that the accretion rate of ER UMa in quiescence is  $7.3 \times 10^{-11} M_\odot/\text{yr}$  for a disk inclination angle of  $50^\circ$ , a  $1.0 M_\odot$  WD and the Gaia distance of 374 pc.

With a distance of 374 pc, and for a WD mass range  $M_{\text{wd}} \approx 1.0 - 1.2 M_\odot$ , we find that during the brief quiescence of only four days, the accretion rate has dropped to  $10^{-10.5} - 10^{-10} M_\odot/\text{yr}$ , while the white dwarf has a temperature of  $30,000 \pm 5000$  K. This accretion rate agrees with DN quiescent mass accretion rates, however, the white dwarf in ER UMa is much hotter ( $\sim 30,000$  K) than other white dwarfs in dwarf novae below the CV period gap which have typical temperatures  $\sim 15,000$  K.

If the white dwarf in ER UMa is heated by compressional heating alone, then the surface temperature during quiescence (Townesley & Bildsten 2003) with an accretion rate of  $2.1 \times 10^{15}$  g/s, is given by

$$T_{\text{eff}} = 1.7 \times 10^4 \text{ K } (< \dot{M} > / 10^{-10})^{0.25} [M_{\text{wd}} / 0.9].$$

Thus, the white dwarf should have  $T_{\text{eff}} = 14,272$  K, a factor of two smaller than from our modeling of ER UMa's FUV spectra in quiescence. For both the low inclination disk models and high inclination disk models, our estimates of the white dwarf surface temperature are a factor of two hotter than the average WD temperature of the white dwarfs in SU UMa systems below the period gap.

The WD during quiescent accretion might be heated not only by compression due to the weight of the accreted gas but also by the boundary layer. If, as expected for low mass accretion rates, the boundary layer is optically thin, then it advects energy directly into the outer layers of the WD and especially in its equatorial region. The broad strong emission lines of C III (977 & 1175 Å), O VI (1131.9 & 1137.6 Å), and also possibly of N IV (921, 924, 941 Å), S VI (933.4 & 944.5 Å) are all indicative of the presence of a very hot component, namely the boundary layer.



## ACKNOWLEDGEMENTS

We are grateful to an anonymous referee for helpful comments on ER UMa. P.G. is pleased to thank William (Bill) P. Blair at the Henry Augustus Rowland Department of Physics and Astronomy at the Johns Hopkins University, Baltimore, MD, for his kind hospitality. This work is supported by the National Aeronautics and Space Administration (NASA) under grant number NNX17AF36G, issued through the Office of Astrophysics Data Analysis Program (ADAP) to Villanova University.

## REFERENCES

- Cannizzo, J. K., & Wheeler, J. C. 1984, *ApJS*, 55, 367  
 Dubus, G., Otulakowska-Hypka M., Lasota J.P., 2018, *A&A*, 617, A26  
 Fitzpatrick, E.L., & Massa, D. 2007, *ApJ*, 663, 320  
 Froning, C.S., Long, K.S., Gänsicke, B.T., & Szkody, P. 2012, *ApJS*, 199, 7  
 Godon, P., Sion, E.M., Levay, K., Linnell, A.P., Szkody, P., Barrett, P.E., Hubeny, I., & Blair, W.P. 2012, *ApJS*, 203, 29  
 Szkody, P., Silber, A., Honeycutt, R.K., Hoard, D.W., Pastwick, L. 1996, in Evans A., Wood J.H. (eds) *Cataclysmic Variables and Related Objects*, *ASSL*, 208, 55  
 Green, R.F., Schmidt, M., Liebert, J., 1986, *ApJS*, 61, 305  
 Harvey, D. A., Skillman D. R., Patterson J., Ringwald F., 1995, *PASP*, 107, 551  
 Hubeny, I. 1988, *Comp. Phys. Commun.*, 52, 103  
 Hubeny, I., & Lanz, T. 1995, *ApJ*, 439, 875  
 Iida, M. 1994, *VSOLJ Variable Star Bulletin*, 19, 2  
 Kato, T. & Kunjaya, C. 1995, *PASJ*, 47, 163  
 Kato, T. et al., 1999, *Universal Academy Press*, Tokyo, p. 45  
 Kato, T. et al., 2018, *PASJ*, pp. 1-126  
 Knigge, C. et al., 2007, *MNRAS*, 373, 484  
 Montgomery, M. M. 2012, *ApJ*, 753, L27  
 Ohshima, T. et al., 2014, *PASJ*, 66, 670  
 Otulakowska-Hypka, M., Olech, A., Patterson, J. 2016, *MNRAS*, 460, 2526  
 Patterson, J., Kemp J., Saad J., Skillman D. R., Harvey D., Fried R., Thorstensen J. R., Ashley R., 1997, *PASP*, 109, 468  
 Patterson, J. 1999, in Mineshige S., Wheeler J. C., eds, *Disk Instabilities in Close Binary Systems*, *Universal Academy Press*, Kyoto, p. 61  
 Patterson, J. et al., 2012, *MNRAS*, 434, 3, pp. 1902  
 Skillman, D. R., Patterson J., Kemp J., Harvey D. A., Fried R. E., Retter A., Lipkin Y., Vanmunster T., 1999, *PASP*, 111, 1281  
 Thorstensen, J.R., Taylor C.J., Becker C.M., Remillard R.A., 1997, *PASP*, 109, 477  
 Wade, R. A., & Hubeny, I. 1998, *ApJ*, 509, 350 (WH98)  
 Wood, M. A., Burke C. J., 2007, *ApJ*, 661, 1042  
 Zemko, P. et al., 2014, *Contrib Astron Obs S*, 43, 319